Spin-polarized electric current in silicene nanoribbons induced by atomic adsorption

C. Núñez,[1,2] P. A. Orellana,[1] L. Rosales,[1] R. A. Römer,[2] and F. Domínguez-Adame[3,2]

[1]*Departamento de Física, Universidad Técnica Federico Santa María, Casilla 110 V, Valparaíso, Chile*
[2]*Department of Physics, University of Warwick, Coventry, CV4 7AL, United Kingdom*
[3]*GISC, Departamento de Física de Materiales, Universidad Complutense, E-28040 Madrid, Spain*

We investigate the nonequilibrium transport properties of a silicene armchair nanoribbon with a random distribution of adsorbed atoms in apex positions. A ferromagnetic insulator grown below the nanoribbon splits spin-up and spin-down electron bands and gives rise to a spin polarization of the conductance. The conductance vanishes when the Fermi energy matches the adatom levels due to the coupling of adatom localized states with the continuum spectra of the nanoribbon. This is the well-known Fano effect, resulting in a spin-dependent antiresonance in the conductance. The different antiresonance energies of spin-up and spin-down electrons give rise to a full spin polarization of the conductance in a broad energy window. This spin-dependent Fano effect opens the possibility to using it in spintronics as a tuneable source of polarized electrons.

I. INTRODUCTION

The field of spintronics is rapidly developing from its roots in magnetic metal multilayers. In recent years, two-dimensional (2D) materials came to the forefront in spintronics and advances in this field are expected to occur based on hybrid systems [1]. Although graphene at present dominates the sector due to its high-electron mobility, a plethora of other novel 2D materials offers fascinating fundamental properties for spin transport and controlled spin-light interaction [2–4]. In this context, silicene is a particularly promising candidate for the design of spintronic devices [5,6]. The two sublattices of the honeycomb lattice in silicene are not coplanar and first-principles calculations suggest that the spin-orbit interaction opens a sizable gap at the Dirac point of the order of 1.55 meV [7].

Half-metals, in which one spin channel is conductive but the other one is insulating or semiconducting, turn out to be a key ingredient to achieve spin-polarized currents. Hybrid structures of 2D materials and ferromagnetic insulators, like EuO, EuS, yttrium iron garnet, or cobalt ferrite, provide a route to induce half-metallicity [8–14] and pave the way for spintronic applications [15–24]. The ferromagnetic insulator induces a proximity exchange interaction between the spins in the magnetic and nonmagnetic material that results in a spin modulation without compromising the crystallinity of the structures [25].

Recently we have proposed a spin-filter device based on a silicene nanoribbon [26]. A ferromagnetic insulator below the nanoribbon gives rise to the spin polarization of the electric current. A random distribution of vacancies causes Anderson localization of electrons. Since the localization length was found to be spin dependent, only electrons with one spin orientation can reach the drain contact because their localization length is larger than the length of the device while electrons with opposite spin are largely back-reflected [26]. Besides vacancies, other types of point defects can affect electron transport in silicene nanoribbons. In particular, metal adatoms present much stronger binding to silicene than to graphene [27] and can induce a transition from semimetallic to semiconducting behavior [28,29] or produce a quantum

anomalous Hall effect [30]. Moreover, chemisorption of a single H atom on silicene induces the formation of a localized state around the adatom, which acts as a resonant scatterer for charge carriers [31]. Hence, a significant reduction of the electron mobility is anticipated since the absence of clustering prevents the conversion of isolated adatoms into clusters, which are known to have a much smaller effect on electron mobility [31].

Theoretical methods and modeling are needed to understand the role of adatoms in the electron transport of silicene and their influence on the spin-filtering capabilities induced by the proximity exchange interaction. In this paper, we address the effects of a random distribution of adatoms on the electron transport properties of narrow silicene nanoribbons. Interestingly, De Padova *et al.* [32] have already synthesized silicene nanoribbons with very large aspect ratio (several nanometers in length and a constant width of about 2 nm). These nanoribbons usually display higher electrical sensitivity to the adsorption of certain molecules, such as CO, at low concentration compared to graphene nanoribbons [33]. The tunnel coupling between adatoms and silicon atoms induces an electronic Fano effect [34] that makes the conductance vanish when the Fermi level matches the resonant energy induced by the adatoms. The resonant energy turns out to be independent of the random distribution of adatoms, provided that they do not cluster. When the nanoribbon is in close proximity to a ferromagnetic insulator, the resonant energy depends on the electron spin and consequently the electric current can be highly spin polarized. Our results expand the base of available materials to designing a tuneable source of polarized electrons for spintronics.

II. THEORETICAL MODEL

The system consists of a narrow silicene nanoribbon of width W and length L connected to source and drain leads, as shown schematically in Fig. 1. In order to avoid topologically protected edge states that appear at the Fermi energy in zigzag nanoribbons [35], we restrict ourselves to nanoribbons with armchair edges hereafter. A ferromagnetic insulator below the nanoribbon induces a spin splitting of the electronic states.
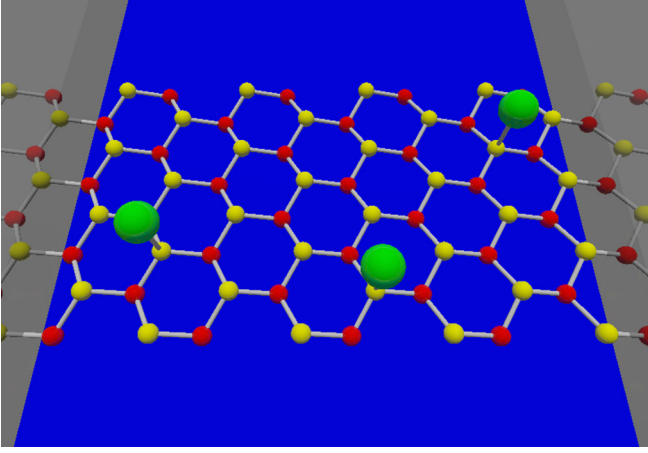
FIG. 1. Schematic view of the device. The armchair silicene nanoribbon is connected to left (L) and right (R) leads, with a ferromagnetic insulator grown below it (shown as the blue region in the figure). A random distribution of adatoms is shown as green spheres. Smaller yellow and red spheres indicate the nonequivalent Si atoms in the silicene nanoribbon.

Consequently, electrons in the nanoribbon will be subject to a positive or negative constant potential, according to their spin.

Electrons in the silicene honeycomb lattice are described by a single π-orbital tight-binding Hamiltonian of the form $H = H_{\mathrm{SN}} + H_{\mathrm{ad}} + H_{\mathrm{tun}} + H_{\mathrm{exc}}$. The Hamiltonian for the electron in the silicene nanoribbon is [36]

$$H_{\mathrm{SN}} = -t \sum_{\langle i,j \rangle \sigma} c_{i\sigma}^{\dagger} c_{j\sigma} + \frac{\lambda_{\mathrm{SO}}}{3\sqrt{3}} \sum_{\langle\langle i,j \rangle\rangle \sigma \tau} v_{ij} c_{i\sigma}^{\dagger} \sigma_z c_{j\tau}, \quad (1)$$

where $c_{i\sigma}^{\dagger}$ ($c_{i\sigma}$) creates (annihilates) an electron at silicon atom i. Sums over $\langle i,j \rangle$ and $\langle\langle i,j \rangle\rangle$ run over nearest and next-nearest neighbor sites, respectively. The spin indices $\uparrow, \downarrow$ are indicated by σ and τ hereafter. The first term corresponds to the nearest neighbor hopping energy $t = 1.6$ eV and the second term represents the spin-orbit coupling with $\lambda_{\mathrm{SO}} = 3.9$ meV, where $v_{ij} = \pm 1$ is the Haldane factor [37] and σ_z is the Pauli matrix. The Hamiltonian corresponding to adatoms levels is given as

$$H_{\mathrm{ad}} = \sum_{j \in \mathcal{L}, \sigma} \varepsilon_{\mathrm{ad}} d_{j\sigma}^{\dagger} d_{j\sigma}, \quad (2)$$

where $d_{j\sigma}^{\dagger}$ ($d_{j\sigma}$) creates (annihilates) an electron at the adatom j, with the index j running over those silicon sites with an attached adatom, denoted by $\mathcal{L}$ above. Adatoms are assumed to occupy apex positions and electrons may tunnel from and to the silicon atom on which the adatom is located. Therefore, the tunnel coupling is expressed as

$$H_{\mathrm{tun}} = t_{\mathrm{ad}} \sum_{j \in \mathcal{L}, \sigma} (c_{j\sigma}^{\dagger} d_{j\sigma} + d_{j\sigma}^{\dagger} c_{j\sigma}), \quad (3)$$

where t_{ad} is the hopping parameter between the adatom and the silicene nanoribbon. Finally, the term

$$H_{\mathrm{exc}} = \sum_{i\sigma} M c_{i\sigma}^{\dagger} \sigma_z c_{i\sigma} \quad (4)$$

describes the spin splitting of electron states due to the proximity exchange interaction with the ferromagnet. It raises

(lowers) the energy levels of spin-up (spin-down) electrons by an amount $+M$ ($-M$) [26].

We study electron transport across the nanoribbon using the Green's function formalism combined with decimation techniques [38,39]. This approach allows us to obtain the transmission coefficient $T_\sigma(E)$ for an electron with energy E and spin σ. Details of the calculations can be found in Ref. [26]. In the linear response regime, the conductance is calculated from the transmission coefficient using the Landauer formula at zero temperature [40],

$$I_\sigma(V, E_F) = \frac{e}{\pi \hbar} \int_{E_F - eV/2}^{E_F + eV/2} T_\sigma(E) dE, \quad (5)$$

where E_F is the equilibrium Fermi energy. For the sake of simplicity, here we assume that the voltage drops across the conductor-electrode interfaces only, although this assumption does not affect significantly the current-voltage characteristics [41]. The total polarization of the spin-dependent linear conductance $G_\sigma(E_F) = I_\sigma(V, E_F)/V$ ($V \to 0$) is defined as

$$P(E_F) = \frac{G_\uparrow(E_F) - G_\downarrow(E_F)}{G_\uparrow(E_F) + G_\downarrow(E_F)}, \quad (6)$$

and it will be the figure of merit to assess the spin-filtering properties of the device.

III. RESULTS

A. Linear conductance in the absence of ferromagnet

Silicene nanoribbons, grown in a controlled environment of gas such as hydrogen, oxygen, boron, lithium, or silver, will be covered by a random distribution of adatoms while possibly retaining their honeycomb structure [29]. Model parameters as the energy level $\varepsilon_{\mathrm{ad}}$ and the tunnel energy t_{ad} will depend on the particular species adsorbed by the nanoribbon. In addition, the fraction c of silicon atoms with an attached adatom will vary according to the growth conditions. Another crucial parameter of the model is the spin splitting M due to proximity exchange interaction with the ferromagnetic insulator. In our simulations we take typical values of these magnitudes to illustrate the feasibility of the proposed device. Other values of the model parameters do not qualitatively change our main conclusions.

In Fig. 2, we show the average conductance $\langle G \rangle / G_0$ as a function of the Fermi energy E_F when the energy level of the adatom is $\varepsilon_{\mathrm{ad}} = 0.10t$ (0.16 eV) and the hopping parameter $t_{\mathrm{ad}} = 0.10t$ (0.16 eV). Here $G_0 = e^2/h$ is the quantum of conductance per spin. Spin-splitting effects are not considered for the moment ($M = 0$). We set the size of the system of the nanoribbons, $W \times L$, as width $W = 2.35$ nm and length $L = 23.22$ nm that were used in all of our calculations. Results for the pristine sample ($c = 0$) are compared to the average over 100 realizations of random samples with concentrations from $c = 0.01$ up to $c = 0.50$. The characteristic quantum plateaus of the conductance are clearly revealed when $c = 0$ but the conductance drops abruptly at the adatom energy $\varepsilon_{\mathrm{ad}}$ at finite values of c. The occurrence of an antiresonance in the conductance can be traced back to quantum interference between the states in the continuum of the nanoribbon and the localized states of the adatoms. This is nothing but the electronic analog of the optical Fano effect [34]. It originates
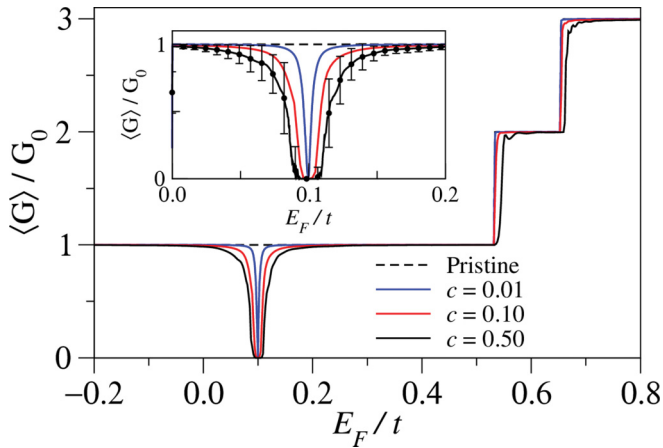
FIG. 2. Average conductance as a function of the Fermi energy of a silicene nanoribbon when $M = 0$. Solid lines correspond to the average over 100 realizations of random samples with adatom concentration $c = 0$ (pristine), 0.01, 0.10, and 0.50. The energy level of the adatom is $\varepsilon_{ad} = 0.10t$ and the hopping parameter $t_{ad} = 0.10t$ with $t = 1.6$ eV. The inset shows an enlarged view of the antiresonance. Only the error bars of the more disordered sample ($c = 0.5$) are displayed for clarity. Fluctuations strongly diminish upon lowering c.

from the interference of two coexisting paths for a traveling electron in the system. One path is a direct way that traverses the nanoribbon while the second path includes a hopping on and off the adatom and then the electron continues with propagation. The destructive interference between these two paths is at the heart of the Fano antiresonance. The conductance around a Fano antiresonance at an energy E_{ar} can be fitted by the general expression $G(E_F)/G_0 \sim (\tilde{\epsilon} + q)^2/(\tilde{\epsilon}^2 + 1)$. Here $\tilde{\epsilon} = (E_F - E_{ar})/\gamma$ corresponds to the normalized energy of the Fano antiresonance, q is an adjustable parameter related to the phase shift originated in the interference phenomena, and γ is an effective coupling between the adatom and the nanoribbon [42,43].

When the concentration of adatoms increases, the antiresonance does not shift but the dip becomes broader. For high concentration of adsorbed atoms, a gap centered at the adatom energy ε_{ad} opens. The antiresonance remains despite having high concentrations of adatoms, and the fully covered nanoribbon ($c = 1$) displays a gap of width t_{ad}^2/t centered at the adatom energy level, as can be demonstrated as follows. The dispersion relation in the pristine nanoribbon is

$$E_0(k_\parallel, k_\perp) = \pm t\sqrt{1 + 4\cos k_\parallel \cos k_\perp + 4\cos k_\perp^2}, \quad (7)$$

where $k_\parallel$ and $k_\perp$ are the longitudinal and transverse wave numbers in units of the inverse of the lattice period, respectively. Here the subscript 0 refers to the absence of adatoms. The energy spectrum is symmetric about $E = 0$ and the two bands touch at this energy if $k_\perp = 2\pi/3$. Then the nanoribbon is metallic and the longitudinal dispersion relation is

$$\varepsilon_0(k_\parallel) \equiv E_0(k_\parallel, k_\perp = 2\pi/3) = \pm 2t|\sin(k_\parallel/2)|. \quad (8)$$

On the other side, in the fully covered nanoribbon ($c = 1$) the energy levels of the Si atoms are renormalized and become energy dependent after the substitution $\varepsilon_{Si} \to \varepsilon_{Si} +$
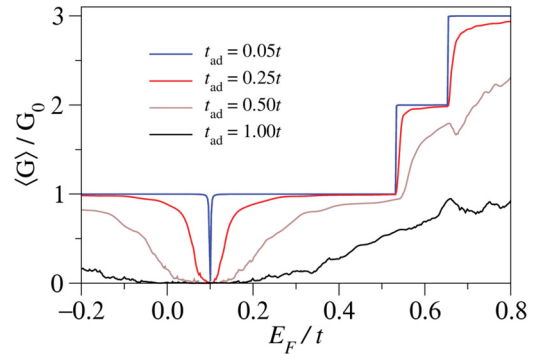

FIG. 3. Average conductance as a function of the Fermi energy of a silicene nanoribbon when $M = 0$. Results were averaged over 100 realizations of random samples with adatom concentration $c = 0.05$ and $t_{ad} = 0.05t$, $0.25t$, $0.50t$, and $1.00t$, where $t = 1.6$ eV. The energy level of the adatom is $\varepsilon_{ad} = 0.10t$.

$t_{ad}^2/[\varepsilon(k_\parallel) - \varepsilon_{ad}]$. Now $\varepsilon(k_\parallel)$ stands for the dispersion relation when $c = 1$. Notice that we have taken $\varepsilon_{Si} = 0$ throughout this work. Introducing this substitution in Eq. (8) yields

$$\varepsilon(k_\parallel) = \frac{t_{ad}^2}{\varepsilon(k_\parallel) - \varepsilon_{ad}} \pm 2t|\sin(k_\parallel/2)|. \quad (9)$$

In this case, a gap opens at $k_\parallel = \pi$. Taking $\varepsilon_{ad} = 0$ for simplicity, the two roots of Eq. (9) at $k_\parallel = \pi$ are found to be $\varepsilon_\pm = \pm t \mp t\sqrt{1 + (t_{ad}/t)^2}$. Consequently, the magnitude of the gap is $|\varepsilon_+ - \varepsilon_-| = 2\sqrt{t^2 + t_{ad}^2} - 2t \simeq t_{ad}^2/t$, where we have taken into account that $t_{ad} \ll t$.

We now turn to the dependence of the antiresonance on the model parameters ε_{ad} and t_{ad}. Figure 3 displays the average conductance $\langle G \rangle$ as a function of the Fermi energy E_F in units of the hopping energy t for different values of t_{ad} when $\varepsilon_{ad} = 0.10t$. Results were averaged over 100 realizations of random samples with adatom concentration $c = 0.05$. The average conductance vanishes at $E_F = \varepsilon_{ad}$ and the antiresonance becomes broader on increasing t_{ad}. It can be shown that the width of the antiresonance scales quadratically with t_{ad}, provided that the adatom concentration is not large. We have also performed calculations when the hopping energy varies at random with mean value t_{ad} from adatom to adatom (not shown in the figure). The general trend is the same as before, in the sense that the larger the fluctuation of the hopping energy, the wider the antiresonance. But even if this hopping is random, the conductance vanishes at $E_F = \varepsilon_{ad}$. Therefore, we come to the conclusion that the Fano antiresonance effect is a very robust phenomenon, which is advantageous for applications.

B. Electric current in the absence of ferromagnet

Figure 4 displays the current-voltage characteristics for different values of the adatom concentration when the Fermi energy at equilibrium is $E_F = 0$. The rest of the parameters are the same as in Fig. 2. The pristine nanoribbon displays a perfectly ohmic current-voltage characteristics over the entire range of voltage V. However, the response becomes nonohmic at finite adatom concentration and an inflection point appears
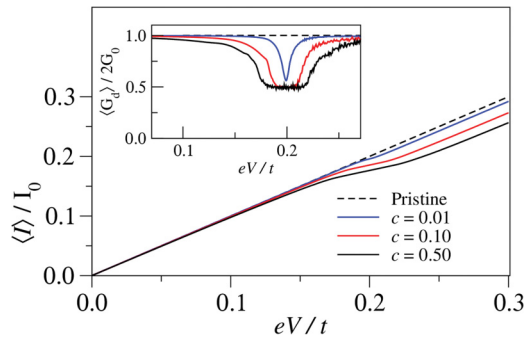
FIG. 4. Electric current through silicene nanoribbons, averaged over 100 realizations of random samples, in units of $I_0 = et/\pi\hbar$, as a function of the source-drain potential energy drop eV, for $E_F = 0$ and the rest of parameters as in Fig. 2. The inset shows the corresponding average differential conductance $\langle G_d \rangle = \langle dI/dV \rangle$, expressed in units of the quantum of conductance $2G_0 = 2e^2/h$.

at $eV = 2\varepsilon_{ad} = 2t$. The point reveals itself as a minimum in the differential conductance, as seen in the inset of Fig. 4. The drop of about 50% of the quantum of conductance $2G_0$ can be easily understood as follows: Assuming that the transmission coefficient does not change much with the applied voltage, one can obtain a simple expression for the differential conductance from the electric current (5). The result is $\langle G_d \rangle/2G_0 \simeq (1/2)[T_\sigma(E_F + eV/2) + T_\sigma(E_F - eV/2)]$. When $E_F = 0$ (as in the inset of Fig. 4), the last term equals unity since the Fano antiresonance lies on the positive-energy side and the nanoribbon is metallic. Thus $\langle G_d \rangle/2G_0 \simeq (1/2)[1 + T_\sigma(eV/2)]$. When $eV/2$ is close to the Fano antiresonance, located at an energy $\varepsilon_{ad} = 0.1$ (i.e., $eV \sim 0.2$), the transmission vanishes and $\langle G_d \rangle/2G_0 \simeq 1/2$. On the contrary, far from the Fano antiresonance, the transmission becomes unity and $\langle G_d \rangle/2G_0 = 1$. Also notice that the gap increases with the adatom concentration, as we anticipated above. Hence, atomic adsorption induces a chemically tunable gap in silicene nanoribbons.

C. Polarization effects of the ferromagnet

As mentioned before, half-metallicity of the system arises as a consequence of the spin splitting induced by the ferromagnetic insulator. We describe the splitting by the parameter M in Eq. (4). *Ab initio* calculations obtain values of the order of 100–200 meV for graphene in close proximity to chalcogenides (EuO and EuS) [44]. Unfortunately, no similar calculations have been carried out in silicene yet and the magnitude of the parameter M is largely unknown. In our numerical simulations, we take a moderate value $M = 100$ meV to be on the safe side, although higher values are expected to result in better performance.

In Fig. 5(a), we show the resulting spin-dependent conductance $\langle G_\sigma \rangle$ ($\sigma = \uparrow, \downarrow$) as a function of the Fermi energy E_F for both spin directions, averaged over 100 realizations of random samples with $c = 0.05$, $c = 0.10$, and $c = 0.50$. The shape of the conductance curve is essentially the same for both spin orientations but blue and red shifted for spin up and spin down by an amount M, respectively. Fano antiresonances are wider than those shown in Fig. 2 for the same adatom concentration
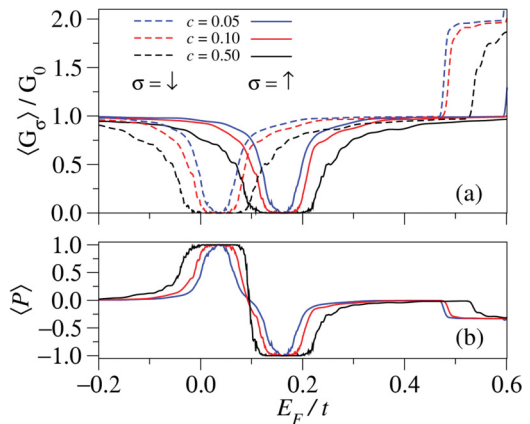

FIG. 5. (a) Spin-up (solid lines) and spin-down (dashed lines) conductances as a function of the Fermi energy of a silicene nanoribbon when $M = 100$ meV, averaged over 100 realizations of random samples with adatom concentrations $c = 0.05$, 0.10, and 0.50. The energy level of the adatom is $\varepsilon_{ad} = 0.10t$ and the hopping parameter $t_{ad} = 0.25t$ with $t = 1.6$ eV. (b) Average conductance polarization as defined by Eq. (6).

because t_{ad} is now larger. We can then take advantage of the abrupt profile of the conductance curves to generate spin-polarized electric current through the silicene nanoribbon, as deduced from the polarization shown in Fig. 5(b). When the Fermi level lies in the vicinity of $\varepsilon_{ad} - M$, the electric current will be fully spin-down polarized. Similarly, when Fermi level approaches $\varepsilon_{ad} + M$, the electric current will become fully spin-up polarized. By increasing the adatom concentration, the plateaus of the polarization around $\varepsilon_{ad} \pm M$ can be made wide enough to ensure thermal stability in device applications, that is, keeping the width of the antiresonance larger than $k_B T$.

IV. CONCLUSIONS

We have studied the electrical conductance of narrow silicene nanoribbons [32] in close proximity to a ferromagnetic insulator. The ferromagnet induces a spin splitting of the energy levels of the silicene nanoribbon. The magnitude of the splitting in silicene is still unknown and the we have used the same value found in graphene grown on chalcogenides [44] to illustrate the phenomenon. We have also investigated the impact of a random distribution of adatoms adsorbed on the nanoribbon. The linear conductance shows clear signatures of the electronic Fano effect due to the coupling of the localized states at the adatoms and the continuum of propagating states in the nanoribbon. The Fano antiresonance becomes spin dependent due to the proximity exchange interaction between the itinerant electrons and the magnetic ions of the ferromagnet. The effect is robust and can be tuned by setting parameters like the adatom concentration. Moreover, it could be used to generate spin-polarized currents for real-world applications in spintronics.

[1] W. Han, APL Mater. **4**, 032401 (2016).

[2] A. Fert, Thin Solid Films **517**, 2 (2008).

[3] H. Zabel, Superlattices Microstruct. **46**, 541 (2009).

[4] V. K. Joshi, Eng. Sci. Technol. Int. J. **19**, 1503 (2016).

[5] Y. Wang, R.-G. Quhe, D.-P. Yu, and J. Lu, Chin. Phys. B **24**, 087201 (2015).

[6] J. Zhao, H. Liu, Z. Yu, R. Quhe, S. Zhou, Y. Wang, C. C. Liu, H. Zhong, N. Han, J. Lu, Y. Yao, and K. Wu, Prog. Mater. Sci. **83**, 24 (2016).

[7] C.-C. Liu, W. Feng, and Y. Yao, Phys. Rev. Lett. **107**, 076802 (2011).

[8] H. Haugen, D. Huertas-Hernando, and A. Brataas, Phys. Rev. B **77**, 115406 (2008).

[9] Y.-L. Lee, S. Kim, C. Park, J. Ihm, and Y.-W. Son, ACS Nano **4**, 1345 (2010).

[10] H. X. Yang, A. Hallal, D. Terrade, X. Waintal, S. Roche, and M. Chshiev, Phys. Rev. Lett. **110**, 046603 (2013).

[11] Z. Wang, C. Tang, R. Sachs, Y. Barlas, and J. Shi, Phys. Rev. Lett. **114**, 016603 (2015).

[12] J. B. S. Mendes, O. Alves Santos, L. M. Meireles, R. G. Lacerda, L. H. Vilela-Leão, F. L. A. Machado, R. L. Rodríguez-Suárez, A. Azevedo, and S. M. Rezende, Phys. Rev. Lett. **115**, 226601 (2015).

[13] P. Wei, S. Lee, F. Lemaitre, L. Pinel, D. Cutaia, W. Cha, F. Katmis, Y. Zhu, D. Heiman, J. Hone, J. S. Moodera, and C.-T. Chen, Nat. Mater. **15**, 711 (2016).

[14] J. C. Leutenantsmeyer, A. A. Kaverzin, M. Wojtaszek, and B. J. van Wees, 2D Mater. **4**, 014001 (2017).

[15] Y. G. Semenov, K. W. Kim, and J. M. Zavada, Appl. Phys. Lett. **91**, 153105 (2007).

[16] P. Michetti and P. Recher, Phys. Rev. B **84**, 125438 (2011).

[17] J. Munárriz, F. Domínguez-Adame, P. A. Orellana, and A. V. Malyshev, Nanotechnology **23**, 205202 (2012).

[18] J. Munárriz, C. Gaul, A. V. Malyshev, P. A. Orellana, C. A. Müller, and F. Domínguez-Adame, Phys. Rev. B **88**, 155423 (2013).

[19] Z. Qiao, W. Ren, H. Chen, L. Bellaiche, Z. Zhang, A. H. MacDonald, and Q. Niu, Phys. Rev. Lett. **112**, 116404 (2014).

[20] E. Díaz, K. Miralles, F. Domínguez-Adame, and C. Gaul, Appl. Phys. Lett. **105**, 103109 (2014).

[21] L. Pietrobon, L. Fallarino, A. Berger, A. Chuvilin, F. Casanova, and L. E. Hueso, Small **11**, 6295 (2015).

[22] M. Saiz-Bretín, J. Munárriz, A. V. Malyshev, and F. Domínguez-Adame, Phys. Lett. A **379**, 2102 (2015).

[23] J. Lee and J. Fabian, Phys. Rev. B **94**, 195401 (2016).

[24] N. Myoung, H. C. Park, and S. J. Lee, Sci. Rep. **6**, 25253 (2016).

[25] A. G. Swartz, P. M. Odenthal, Y. Hao, R. S. Ruoff, and R. K. Kawakami, ACS Nano **6**, 10063 (2012).

[26] C. Núñez, F. Domínguez-Adame, P. A. Orellana, L. Rosales, and R. A. Römer, 2D Mater. **3**, 025006 (2016).

[27] X. Lin and J. Ni, Phys. Rev. B **86**, 075440 (2012).

[28] F. Ersan, Ö. Arslanalp, G. Gökoğlu, and E. Aktürk, Appl. Surf. Sci. **311**, 9 (2014).

[29] Y. Du, J. Zhuang, H. Liu, X. Xu, S. Eilers, K. Wu, P. Cheng, J. Zhao, X. Pi, K. W. See, G. Peleckis, X. Wang, and S. X. Dou, ACS Nano **8**, 10019 (2014).

[30] X.-L. Zhang, L.-F. Liu, and W.-M. Liu, Sci. Rep. **3**, 2908 (2013).

[31] M. Pizzochero, M. Bonfanti, and R. Martinazzo, Phys. Chem. Chem. Phys. **18**, 15654 (2016).

[32] P. De Padova, C. Quaresima, C. Ottaviani, P. M. Sheverdyaeva, P. Moras, C. Carbone, D. Topwal, B. Olivieri, A. Kara, H. Oughaddou *et al.*, Appl. Phys. Lett. **96**, 261905 (2010).

[33] T. H. Osborn and A. A. Farajian, Nano Res. **7**, 945 (2014).

[34] U. Fano, Phys. Rev. **124**, 1866 (1961).

[35] L. Brey and H. A. Fertig, Phys. Rev. B **73**, 235411 (2006).

[36] M. Ezawa, New J. Phys. **14**, 033003 (2012).

[37] F. D. M. Haldane, Phys. Rev. Lett. **61**, 2015 (1988).

[38] C. J. Lambert and D. Weaire, Phys. Status Solidi B **101**, 591 (1980).

[39] S. Datta, *Electronic Transport in Mesoscopic Systems* (Cambridge University Press, Cambridge, UK, 1995).

[40] R. Landauer, Philos. Mag. **21**, 863 (1970).

[41] J. H. Ojeda, M. Pacheco, L. Rosales, and P. A. Orellana, Org. Electron. **13**, 1420 (2012).

[42] M. R. Rezapour, A. C. Rajan, and K. S. Kim, J. Comput. Chem. **35**, 1916 (2014).

[43] M. D. Petrović and F. M. Peeters, Phys. Rev. B **91**, 035444 (2015).

[44] A. Hallal, F. Ibrahim, H. X. Yang, S. Roche, and M. Chshiev, 2D Mater. **4**, 025074 (2017).